Temporal and spatial modulation of Rho GTPases during in vitro formation of capillary vascular network: Adherens junctions and myosin light chain as targets of Rac1 and RhoA

THE JOURNAL OF BIOLOGICAL CHEMISTRY
Vol. 278, No. 50, Issue of December 12, pp. 50702–50713, 2003
Printed in U.S.A.

Temporal and Spatial Modulation of Rho GTPases during *in Vitro* Formation of Capillary Vascular Network

ADHERENS JUNCTIONS AND MYOSIN LIGHT CHAIN AS TARGETS OF Rac1 AND RhoA*

Received for publication, July 7, 2003, and in revised form, August 29, 2003
Published, JBC Papers in Press, September 12, 2003, DOI 10.1074/jbc.M307234200

Ilaria Cascone‡§¶‖, Enrico Giraudo‡§¶, Francesca Caccavari‡§, Lucia Napione‡§, Elisa Bertotti‡§, John G. Collard‡‡, Guido Serini‡§, and Federico Bussolino‡§ §§**

From the ‡Division of Molecular Angiogenesis, Institute for Cancer Research and Treatment (IRCC), the §Department of Oncological Sciences, University of Turin School of Medicine, 10060 Candiolo, Italy, and ‡‡The Netherlands Cancer Institute, 1066 Amsterdam, The Netherlands

Endothelial cells (ECs) self-organize into capillary networks when plated on extracellular matrix. In this process, Rho GTPases-mediated cytoskeletal dynamics control cell movement and organization of cell-to-matrix and cell-to-cell contacts. Time course analysis of RhoA and Rac1 activation matches specific morphological aspects of nascent pattern. RhoA-GTP increases early during EC adhesion and accumulates at sites of membrane ruffling. Rac1 is activated later and localizes in lamellipodia and at cell-to-cell contacts of organized cell chains. When ECs stretch and remodel to form capillary structures, RhoA-GTP increases again and associates with stress fibers running along the major cell axis. N17Rac1 and N19RhoA mutants impair pattern formation. Cell-to-cell contacts and myosin light chains (MLC) are targets of Rac1 and RhoA, respectively. N17Rac1 reduces the shift of β-catenin and vascular endothelial cadherin to Triton X-100-insoluble fraction and impairs β-catenin distribution at adherens junctions, suggesting that Rac1 controls the dynamics of cadherin-catenin complex with F-actin. During the remodeling phase of network formation, ECs show an intense staining for phosphorylated MLC along the plasma membrane; in contrast, MLC is less phosphorylated and widely diffused in N19RhoA ECs. Both N17Rac1 and N19RhoA have been used to investigate the role of wild type molecules in the main steps characterizing in *vitro* angiogenesis: (i) cell adhesion to the substrate, (ii) cell movement, and (iii) mechanical remodeling of matrix. N17Rac1 has a striking inhibitory effect on haptotaxis, whereas N19RhoA slightly inhibits EC adhesion and motility but more markedly Matrigel contraction. We conclude that different Rho GTPases control distinct morphogenetic aspects of vascular morphogenesis.

To distribute nutrients throughout the body, vertebrates have evolved a branching blood vascular system that terminates in a network of size-invariant units, namely capillaries. The development of capillary networks characterized by typical intercapillary distances ranging from 50 to 300 μm is instrumental for optimal metabolic exchange (1). In embryo, homogeneous vascular networks form by vasculogenesis and are remodeled through angiogenesis (2). Both processes require that ECs[1] or their mesodermic precursors, angioblasts, move, proliferate, and then change their shape folding into capillaries. The ability to form networking capillary tubes is a cell autonomous property of ECs and requires permissive extracellular cues such as growth factors, autacoids, signals coming from the extracellular matrix, and physical forces (2–4).

It is well known that culturing ECs on a tridimensional scaffold of extracellular matrix protein markedly accelerates their morphological differentiation in geometric tubular networks (5–8), which are almost identical to vascular beds formed by vasculogenesis *in vivo* (9) or to some anatomical districts by angiogenesis (10–12). When this process occurs on Matrigel, a natural basal membrane matrix, it is rapid (6–16 h), does not require cell proliferation, and is mainly characterized by cell motility and shape rearrangement, which imply dramatic changes in EC cytoskeletal dynamics and adhesive behavior (7, 13).

In the last few years it has been widely demonstrated that Rho GTPases are major regulators of cell polarization and motility. In fibroblasts, Cdc42 mediates filopodia extension and Rac1 both lamellipodia formation and membrane ruffling, and RhoA controls stress fiber formation (14). Both Rac1 and RhoA also participate in the ruffling phenomena of ECs (15). However, GTPase activities exert antagonistic effects in the regulation of different steps of cell motility (14, 16) and show discrete subcellular localizations (17–19). Recent evidence (23–26) suggests that Rho GTPases are part of the signaling pathways triggered by angiogenic inducers (20–22) and regulate the shape of ECs.

We analyzed the temporal and spatial activation of Rac1 and RhoA during capillary vascular network formation by ECs and

* This work was supported in part by Associazione Italiana per la Ricerca sul Cancro, Istituto Superiore di Sanità (IV Programma Nazionale di Ricerca sull'AIDS-2001 and Progetto "Tumor Therapy"), Compagnia di San Paolo, Ministero dell'Istruzione, dell'Università e della Ricerca (60% and PRIN 2002), CNR (Progetto Strategico Oncologia), and FIRB (Project "Ingegneria Tissutale"). The costs of publication of this article were defrayed in part by the payment of page charges. This article must therefore be hereby marked "*advertisement*" in accordance with 18 U.S.C. Section 1734 solely to indicate this fact.

¶ Both authors contributed equally to this work and should be considered as first authors.

‖ Fellow of Fondazione Italiana per la Ricerca sul Cancro (Milano, Italy).

** Fellow of "Comitato Gigi Ghiotti" (Torino, Italy).

§§ To whom correspondence should be addressed: IRCC, Strada Provinciale 142, Km 3.95, 10060 Candiolo (Torino), Italy. Tel.: 390119933347; Fax: 390119933524; E-mail: federico.bussolino@ircc.it.

[1] The abbreviations used are: ECs, endothelial cells; Ab, antibody; BSA, bovine serum albumin; FITC, fluorescein isothiocyanate; GFP, green fluorescence protein; GST, glutathione *S*-transferase; mAb, monoclonal Ab; MLC, myosin light chain; MLC-P, phosphorylated-MLC; PBS, phosphate-buffered saline; RBD, rhotekin binding domain; TRITC, tetramethylrhodamine isothiocyanate; Ve-cadherin, vascular endothelial-cadherin; VEGF, vascular endothelial growth factor; WBD, Wiskott-Aldrich syndrome protein binding domain; FCS, fetal calf serum; PBD, Pak 1B binding domain.

show that their spatially and temporally regulated activation was required for proper formation of such a network. By employing dominant negative molecules, we found that Rac1 and RhoA, respectively, regulate the early formation of adherens junction, among ECs that at the beginning self-organize into clusters and chains, and the phosphorylation level of myosin light chain (MCL) when ECs start stretching to remodel the vascular network.

EXPERIMENTAL PROCEDURES

Reagents—Glutathione *S*-transferase (GST)-Pak 1B binding domain (amino acids 56–141) (GST-PBD), GST-rhotekin binding domain (GST-RBD) (amino acids 1–90), and GST-Wiskott-Aldrich syndrome protein binding domain (WBD) (amino acids 201–321) (GST-WBD) fusion proteins were produced and purified as described (27). GST-PBD, GST-RBD, and GST-WBD bind the GTP-bound form of Rac1 and Cdc42, RhoA, and Cdc42, respectively (28–31). cDNA of N17Rac1, N17cdc42, and N19RhoA dominant negative molecules (kindly provided by G. Bockoc, University of San Diego, San Diego, CA; Dr. A. Hall, University of London, London, UK; and Dr. G. Scita, European Institute of Oncology, Milano, Italy) (32–34) were subcloned into the BamHI/EcoRI site of Pinco retroviral vector (35) and expressed under the control of the two long terminal repeats. Green fluorescence protein (GFP) cDNA was under the control of cytomegalovirus promoter. cDNA of RacQ61L (Rac1QL) and RhoQ63L (RhoAQL) (36, 37) were subcloned into the HindIII/NotI site of Pinco. GST-RBD and GST-PBD cDNAs were respectively subcloned into BamHI/EcoRI sites of pGEX2TK and BamHI/EcoRI sites of pGEX3X and expressed as fusion proteins in *Escherichia coli* BL21 cells. Cells carrying GST-PBD, GST-RBD, or GST-WBD were respectively lysed by sonication in 50 mM Tris-HCl, pH 7.5, containing 100 mM NaCl, 1% Triton X-100, 2 mM dithiothreitol, 5% glycerol, and protease inhibitors (1 mM phenylmethylsulfonyl fluoride, 50 μg/ml leupeptin, 10 μg/ml aprotinin, 5 μg/ml pepstatin). Lysates were purified by affinity chromatography with glutathione-coupled Sepharose 4B beads (Amersham Biosciences). For pull-down assays, beads were extensively washed six times in 50 mM Tris-HCl, pH 7.5, containing 150 mM NaCl, 0.5% Triton X-100, 5 mM $MgCl_2$, and 1 mM dithiothreitol and stored at −80 °C in the presence of 10% glycerol. For immunofluorescence studies of localization of Rac1-GTP, RhoA-GTP, and Cdc42-GTP, GST-PBD and GST-WBD were eluted with 50 mM Tris-HCl, pH 8.0, containing 100 mM NaCl, 2 mM dithiothreitol, 5% glycerol, 20 mM reduced glutathione, and protease inhibitors. GST-RBD was eluted with the same buffer containing 50 mM NaCl. GST fusion proteins were stored at −80 °C.

All indicated monoclonal (mAb) and polyclonal antibody (Ab) were provided by Pharmingen (BD Biosciences) (mAb anti-Rac1, fluorescein isothiocyanate (FITC), and tetramethylrhodamine isothiocyanate (TRITC) conjugated-secondary Abs) and by Santa Cruz Biotechnology (Santa Cruz, CA) (mAb and Ab anti-RhoA, Ab anti-Cdc42, mAb and Ab anti-GST, mAb anti-β-catenin, Ab anti-α-catenin, Ab anti-IQGAP1, mAb anti-β-tubulin). mAbs anti-phosphorylated-MLC (MLC-P) and anti-vascular endothelial (Ve)-cadherin were obtained from Dr. S. Komatsu (University of Massachusetts, Worcester, MA) and Prof. E. Dejana (Institute of Molecular Oncology, Milan, Italy), respectively. Other products were purchased from Sigma.

Cell Culture—Human dermal capillary ECs (Biotech, BD Biosciences) were cultured according to the manufacturer's instructions. EC infection was performed as described previously (38). Briefly, N17Rac1, N17Cdc42, N19RhoA, RhoAQL, and Rac1QL cDNAs subcloned into Pinco vector were transiently transfected into Phoenix packaging cells, and the supernatants were used to infect ECs. As control of infection, GFP analysis was performed both through fluorescence microscope and fluorescence-activated cell sorting (FACS Advantage SE, Biotech, BD Biosciences, San Jose, CA) giving 85–90% of positive ECs. The expression of transgene molecules was evaluated by Western blot analysis and always gave an increase of proteins recognized by specific mAbs anti-Rac1, anti-RhoA, and Ab anti-Cdc42 or as compared with ECs infected with vector alone (not shown). Infection conditions *per se* were without effect on EC morphology and on cell cycle analyzed by propidium iodide fluorescence by FACS flow cytometer.

In Vitro Angiogenesis—To analyze *in vitro* angiogenesis, glass coverslips (2 cm^2 growth area) were coated with 0.25 ml of Matrigel (8.8 mg/ml; Biotech, BD Biosciences), which was immediately aspirated, and the remaining film was allowed to solidify. ECs (125 cells/mm^2) were incubated at 37 °C in a 5% CO_2 humidified atmosphere for 14 h on glass coverslips and observed with an inverted photomicroscope (model DM IRB HC; Leica Microsystems, Solms, Germany). Phase contrast snap photographs and 12–14-h long movies (one frame every 5 min) were taken with a cooled digital CCD Hamamatsu ORCA camera (Hamamatsu Photonics Italy, Milano, Italy), recorded, and analyzed with ImageProPlus 4.0 imaging software to count the number of capillaries/mm^2 (Media Cybernetics, Carlsbad, CA) (39).

In the sprouting assay capillary ECs carrying vector alone or N17Rac1 or N19RhoA were suspended at a density of 4 cells/μl in culture medium containing 20% of Methocel stock (6 g of carboxymethylcellulose in 500 ml of M199) in M199 containing 20% FCS, 0.1 mg/ml porcine heparin. Eight hundred cells were seeded into non-adherent round-bottomed 96-well plates (Falcon, BD Biosciences), and cultured overnight at 37 °C (5% CO_2, 100% humidity). The spheroids were harvested by gently pipetting them and were centrifuged at 300 × *g* for 15 min. The EC spheroids were suspended in 200 μl of M199 medium containing 40% FCS, 1.2% (v/w) methylcellulose with or without 30 ng/ml vascular endothelial growth factor (VEGF)-A_{165} (R&D Systems, Minneapolis, MN), and mixed with an equal volume of diluted collagen solution (7 volumes of collagen from rat tail, 1 volume of 10× M199, 1 volume of 0.1 N NaOH, and 1 volume of 0.2 M Hepes, pH 7.3) (39). After 24 h spheroid photographs were taken with digital CCD Hamamatsu ORCA camera linked to an inverted photomicroscope (model DM IRB HC, Leica).

Biochemical Assays during in Vitro Angiogenesis—Capillary ECs, ECs carrying vector alone, N17Rac1, or N19RhoA (9×10^6) were seeded on 100-mm Petri dishes coated with 9 ml of Matrigel, which was immediately aspirated. Cells were incubated at 37 °C for the indicated times, and after washing with cold PBS, pH 7.4, cells were treated with 8 ml of MatriSperse Cell Recovery Solution (Biotech, BD Biosciences) at 4 °C for 2 h. After complete release from the gel, ECs were centrifuged at 500 × *g* for 5 min at 4 °C.

To analyze the GTP-bound form of Rho GTPases, cells were lysed for 20 min on ice in 50 mM Tris, pH 7.4, 2 mM $MgCl_2$, 100 mM NaCl, 1% Nonidet P-40, 10% glycerol supplemented with protease inhibitors. Lysates were centrifuged for 5 min at 13,000 × *g*, and equal amounts of proteins (500 μg) were incubated with 30 μg of GST-RBD, GST-PBD, or GST-WBD G-Sepharose beads coupled for 60 min at 4 °C. At the end of incubation, beads were washed with the same buffer, and solubilized proteins were resolved on SDS-PAGE (12%), transferred onto polyvinylidene difluoride membranes (Immobilon, Millipore Corp., Bedford, MA), probed with mAbs anti-RhoA, anti-Rac1, or Ab anti-Cdc42, and detected by enhanced chemiluminescence techniques (Amersham Biosciences). Total cell lysates were treated in the same conditions to evaluate the total amounts of RhoA, Rac1, and Cdc42.

To detect phosphorylated MLC (MLC-P), ECs were washed twice with cold PBS containing 1 mM $NaOV_4$ and then immediately boiled in 1 ml of 20 mM Tris, 22 mM glycine, 10 mM dithiothreitol, 1% SDS. Proteins were separated by SDS-PAGE (12%) and immunoblotted with mAb anti-MLC-P.

To analyze Ve-cadherin-catenin complexes, ECs were washed twice with Ca^{2+}- and Mg^{2+}-containing PBS and lysed in 10 mM Tris-HCl, 150 mM NaCl, 2 mM $CaCl_2$, pH 7.5, 1% Nonidet P-40, 1% Triton X-100, and protease inhibitors for 20 min on ice. Lysates were centrifuged for 15 min at 14,000 × *g*. The supernatants were incubated with protein G-Sepharose (Amersham Biosciences) and a mAb anti-β-catenin for 2 h at 4 °C. Then beads were washed with lysis buffer. Pellets were solved in SDS buffer (1% Triton X-100, 1% Nonidet P-40, 0.5% SDS in Ca^{2+}- and Mg^{2+}-containing PBS) and boiled for 5 min. Solubilized proteins were separated by SDS-PAGE (8%) and transferred onto nitrocellulose (Bio-Rad). Nitrocellulose was blocked with 10% BSA in Ca^{2+}- and Mg^{2+}-containing PBS and immunoblotted with mAbs anti-Ve-cadherin or anti-β-catenin, or Abs anti-α-catenin, or anti-IQGAP1. Cell apoptosis was evaluated by Annexin V staining as described (40). Where shown, densitometry was performed with Phoretix 1D software (Nonlinear USA Inc., Durham, NC).

Adhesion Assay—96-Well plates were coated with 1.28 μg/μl Matrigel for 3 h at 37 °C, washed, and blocked with 3% BSA for 2 h at 37 °C. 1×10^4 capillary ECs carrying vector alone or N17Rac1 or N19RhoA were plated to adhere for 30 min. Attached cells were fixed and stained by crystal violet, and the absorbance was read at 540 nm in microtiter plate spectrophotometer (HT6 7000 Bio Assay Reader, PerkinElmer Life Sciences).

Motility Assay—24-Well transwell chambers (Falcon, BD Bioscience Biotech) containing polycarbonate filters with 8-mm pores were used. The underside of the filters were coated with 1.28 μg/μl Matrigel for 1 h at 37 °C and saturated in 3% BSA for 1 h at 37 °C. Two hundred microliters of cell suspension containing 3×10^4 capillary ECs carrying vector alone or N17Rac1 or N19RhoA were plated in the upper cham-

bers of transwell apparatus, and M199 supplemented with 10% FCS was added to the lower chamber. Cells were incubated for 3 h at 37 °C in a 95% air, 5% CO_2 atmosphere. After washing with PBS, the cells migrated to the bottom side of the transwell membrane were fixed with 3.7% glutaraldehyde, and cells on the upper side of the filter were carefully removed by scraping with the edge of a cotton swab. Migrated cells were stained with crystal violet, and the absorbance was read at 540 nm in microtiter plate spectrophotometer. Absorbance values were linear from 1×10^2 to 2×10^4 cells.

Gel Contraction—Gel contraction assay was performed as described previously (41). Capillary ECs (200 cells/mm^2) carrying vector alone or N17Rac1 or N19RhoA were plated as detailed above. Cells were incubated at 37 °C in a 5% CO_2 humidified atmosphere until they spread. In some experiments 100 nM cytochalasin D or 5 μM Y-27632 (Calbiochem) were added from the beginning of incubation. To control the numbers of cell spread on Matrigel, ECs were recovered by using of MatriSperse Cell Recovery Solution and counted. To initiate Matrigel contraction, polymerized gels were gently released from the underlying culture dish. The degree of Matrigel contraction was determined after 14 h by recording pictures with a digital camera (½ inch CCD, JVC) connected to a Stereomicroscope Olympus SZX9 (Olympus Europe, Hamburg, Germany). The gel area was calculated by Image Pro Plus 4x software.

Cell Dissociation Assay—Confluent cultured ECs were treated with 0.01% trypsin in Hepes-buffered saline (1 mM $CaCl_2$, 1.3 M NaCl, 50 mM KCl, 3.3 mM Na_2HPO_4-$7H_2O$, 55 mM glucose, 100 mM Hepes, pH 7.4) (TC treatment) or in Hepes-buffered saline without Ca^{2+} supplemented with 1 mM EGTA (TE treatment) for 15 min at 37 °C and dissociated through 10 times pipetting. The extent of dissociation cells was represented by the index N_{TC}/N_{TE}, where N_{TC} and N_{TE} are the number of clusters and single cells, respectively (42).

Immunofluorescence—Cells cultured on glass coverslips coated with Matrigel were fixed for 30 min in 4% paraformaldehyde in PBS, pH 7.5, quenched with 20 mM NH_4Cl for 30 min, permeabilized with 0.1% saponin in PBS for 30 min on ice, and rinsed twice in PBS. Blocking incubations were performed in PBS containing 10% goat serum and 0.25% fish skin gelatin (1 h, at room temperature). GST-PBD, GST-RBD, or GST-WBD (30 μg) were diluted in 10% of blocking solution and incubated for 1 h at room temperature or overnight at 4 °C. Cells were extensively washed with PBS and then incubated for 30 min at 37 °C with a mAb anti-GST. After washes they were incubated with the secondary FITC-conjugated Ab. In order to exclude interferences of cell fixation on the GTP-bound state of Rho GTPases, pull-down assay was performed on cells fixed, permeabilized, and isolated from Matrigel as detailed above.

Fixed and permeabilized cells were also incubated with mAbs anti-Ve-cadherin, anti-β-catenin, anti-MLC-P, and anti-GST or Abs anti-RhoA or anti-Rac1, and then visualized with secondary TRITC-conjugated and FITC-conjugated Abs.

For F-actin staining, cells were incubated for 30 min at 37 °C with FITC-conjugated phalloidin. ECs infected with a modified Pinco vector without GFP were used for double staining experiments.

RESULTS

Morphological Events of Capillary EC Morphogenesis—Time-lapse video microscopy over a period of 14 h shows that *in vitro* vascular network formation by capillary ECs follows specific and peculiar morphological phases (Fig. 1). During the first 30 min, ECs randomly plated on Matrigel spread, moved, and started to form small and seldom interconnected clusters. After 1 h, ECs were completely spread and clusters increased in size and highly connecting among them. These changes became more evident after 2 h, when discrete Matrigel areas were empty and surrounded by EC islets or chains. Four hours after plating, endothelial chains begun stretching and ECs appeared very elongated. This process continued for another 2 h and was accompanied by a reduction in size of cell clusters and the delineation of polygonal spaces whose dimensions were similar to those observed at the end of the process. During the last 8 h EC chains became progressively thinner, and by 14 h these chains gave rise to EC cords interconnected with nodes that originated from the reduction in size of clusters and their compression.

Activation and Cellular Localization of Rho GTPases during Capillary EC Morphogenesis—Because cell motility largely depends on the control of the actin cytoskeletal dynamics by the Rho GTPase family (14), we studied the time courses of RhoA, Rac1, and Cdc42 activation and their intracellular localization in ECs during vascular network formation Matrigel. To analyze the enzyme GTP-bound state of Rac1, RhoA, and Cdc42 in capillary EC lysates (27), pull-down experiments were performed by using fusion proteins between GST and the Cdc42/Rac interactive binding domain of human PAK1B (GST-PBD), or the Rho binding domain of the Rho effector rhotekin (GST-RBD), or the Cdc42/Rac interactive binding domain of the Wiskott-Aldrich syndrome protein (GST-WBD), which binds specifically to active Cdc42 (31).

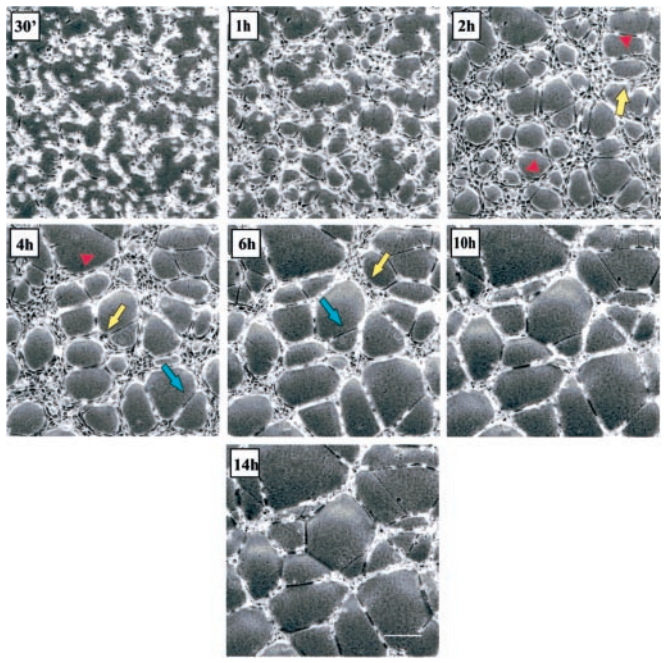

FIG. 1. **Capillary network formation.** Human capillary ECs were plated (125 cells/mm^2) on Matrigel, and the time course of network formation was analyzed by time-lapse video microscopy of a 4-mm^2 wide portion of surface. *Yellow arrows* mark cell clusters; *red arrows* mark cell chains, and *blue arrows* mark the stretched EC chains. This picture is representative of three independent experiments. ×100 magnification; *bar,* 10 μm.

When ECs were put in suspension the amount of RhoA-GTP was very low. Thirty min after plating ECs on Matrigel, RhoA-GTP markedly increased and remained elevated up to 1 h (Fig. 2*A*). After 2 and 4 h, RhoA-GTP decreased, but it was again detectable at 6 h, reaching its maximum at 10 h and subsequently declining again (Fig. 2*A*). Rac1-GTP was detected in suspended cells and increased 2 h after plating, remaining elevated up to 4 h (Fig. 3*A*). Then Rac-GTP progressively decreased and was lower than the basal level after 14 h. The amount of Cdc42-GTP slightly increased in adhering cells as compared with suspended cells but did not change over the time of network formation, including the early step when Rac1 was activated (Fig. 3*C*). This observation suggested that modulation of Cdc42 activation was not essential in our experimental model.

To gain insights into the subcellular localization of Rho GTPases, permeabilized cells were incubated with either GST-PBD, GST-RBD, or GST-WBD, which were then detected by indirect immunofluorescence with an anti-GST Ab. Permeabilization and fixation procedures in the presence of paraformaldehyde did not interfere in the association of Rho GTPase GTP-bound forms with their effectors, as inferred by pull-down experiments performed after capillary EC fixation and permeabilization (Fig. 4). However, this is only a qualitative analysis,

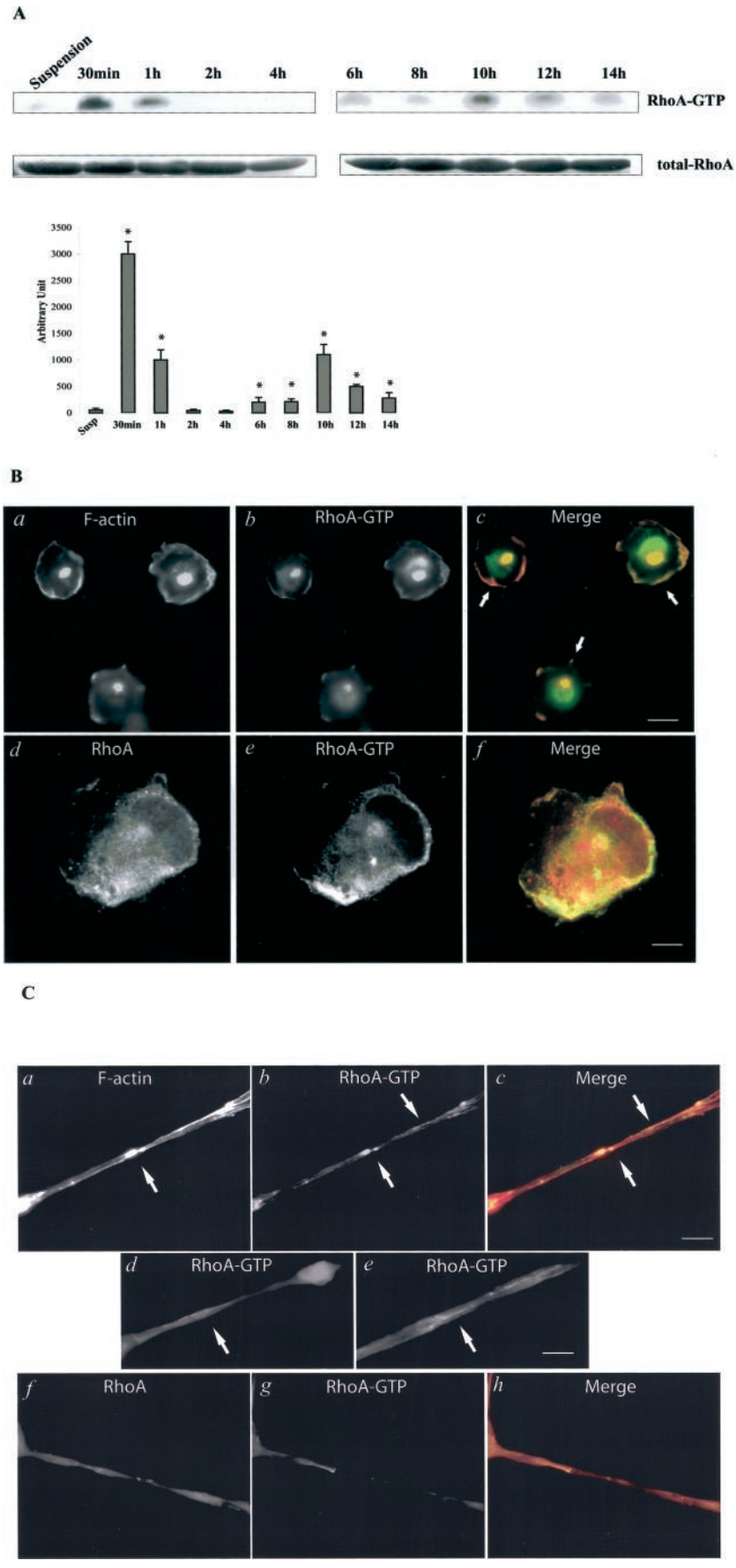

FIG. 2. **Activation of RhoA during capillary EC morphogenesis.** *A*, RhoA-GTP amount was evaluated by pull-down experiments with GST-RBD along the capillary network formation. At the indicated stage of the morphogenetic process on Petri dishes (100 mm diameter; 9×10^6 cells), ECs were dispersed with MatriSperse Cell recovery solution, lysed, and incubated with GST-RBD. Proteins were separated by SDS-PAGE (12%) and then analyzed for bound RhoA molecules by Western blotting. An aliquot of lysate was used for analyzing the total amounts of RhoA. The time courses from 30 min to 4 h and from 6 to 14 h have been performed in separated experiments. Densitometric analysis of three independent experiments is shown as mean ± S.D. *Bars* correspond to time points of the pull-down experiment. Data were analyzed by one-way analysis of variance ($p < 0.0002$) and Student-Newman-Keuls test (* indicates $p < 0.05$ *versus* suspended cells). *B*, subcellular localization of RhoA-GTP after 30 min from the beginning of the morphogenetic process. ECs were fixed and permeabilized, and F-actin was stained with TRITC-phalloidin (*a*) or incubated with Ab anti-RhoA, which was stained by a TRITC anti-rabbit IgG (*d*). RhoA-GTP was localized by incubating the cells with GST-RBD followed by an anti-GST mAb, which was stained by an anti-mouse FITC-IgG (*b* and *e*). The images were merged (*c* and *f*) showing the sites of co-localization of RhoA-GTP with F-actin (*arrows* in *c*) and the distribution of RhoA-GTP compared with total RhoA (*f*). *Bar*, 10 μm. *C*, subcellular localization of RhoA-GTP after 10 h from the beginning of the morphogenetic process. Cells were stained with TRITC-phalloidin (*a*) or with Ab anti-RhoA (*f*). RhoA-GTP was immunodetected in *b*, *d*, *e*, and *g*. The images (*a* and *b*) and (*f* and *g*) were respectively merged showing the sites of co-localization of RhoA-GTP with F-actin (*arrows* in *c*) and the distribution of RhoA-GTP compared with total RhoA (*h*). *Arrows* in *b* show the RhoA-GTP at the cell-cell junction and along the major cell axis. *Arrows* in *d* and in *e* show the accumulation of Rho-GTP near cell-to-cell adhesion sites at higher magnification. *Bar*, 10 μm. These panels are representative of at least four experiments obtained with similar results.

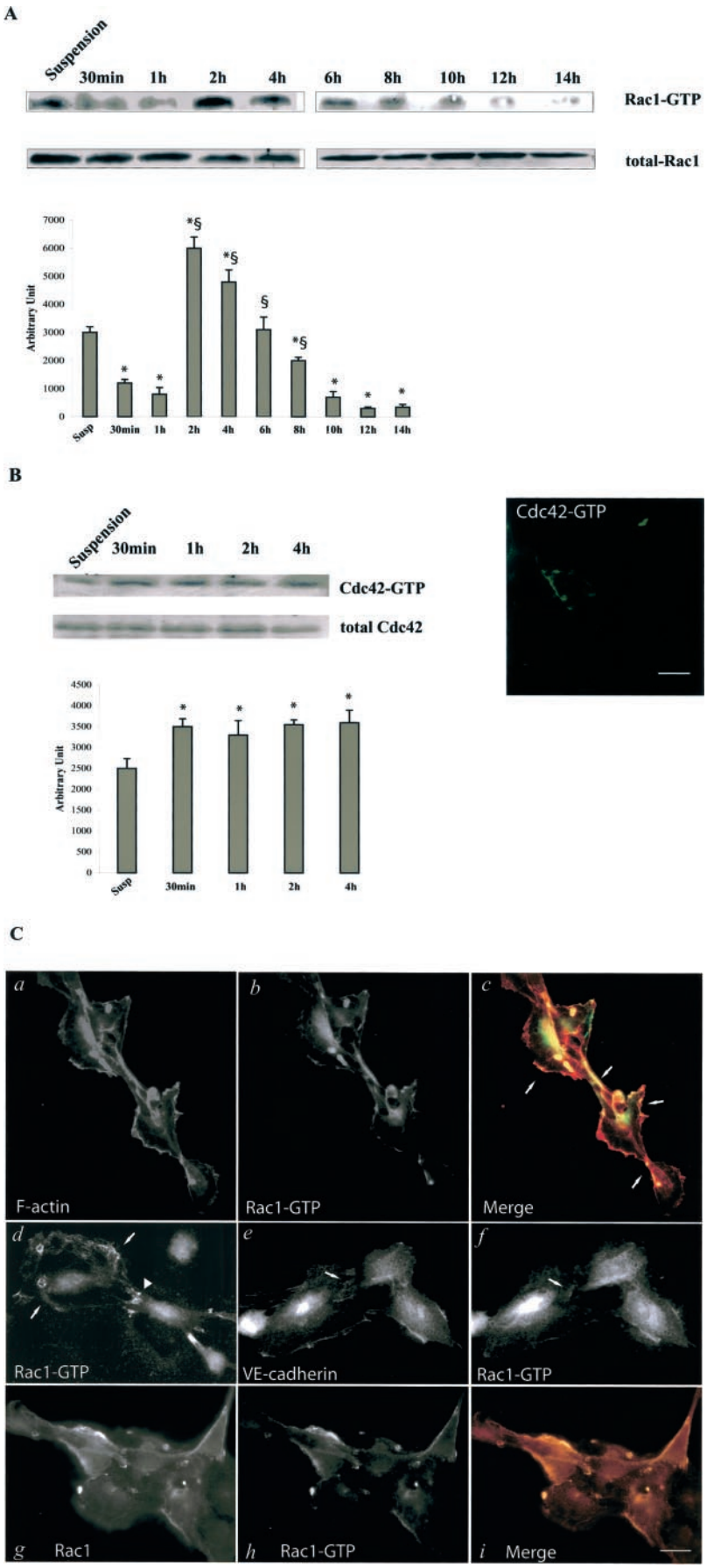

FIG. 3. **Activation of Rac1 during capillary EC morphogenesis.** *A* and *B*, the amount of Rac1-GTP and Cdc42-GTP was evaluated by pull-down experiments, respectively, with GST-PBD and GST-WBD along the capillary network formation as specified in Fig. 1. Densitometric analysis of three independent experiments is shown as mean ± S.D. *Bars* correspond to time points of the pull-down experiment. Data were analyzed by one-way analysis of variance (Rac1 pull-down, $p < 0.0005$; Cdc42 pull-down, $p < 0.001$) and Student-Newman-Keuls test (* and § indicate $p < 0.05$ *versus* suspended cells and cells plated for 30 min, respectively). *B*, Cdc42-GTP staining in ECs after 2 h from the beginning of the morphogenetic process is shown. Cdc42-GTP was localized by incubating the cells with GST-WBD and stained as detailed in the legend to Fig. 2. *C*, subcellular localization of Rac1-GTP after 2 h from the beginning of the morphogenetic process. ECs were fixed and permeabilized, and F-actin cytoskeleton was stained with TRITC-phalloidin (*a*). Total Rac1 was detected by Ab anti-Rac1, which was stained by a TRITC anti-rabbit IgG (*g*). Rac1-GTP (*b*, *d*, *f*, and *h*) was localized by incubating the cells with GST-PBD and stained as detailed in the legend to Fig. 2. *d*, *arrow* and *arrowhead* show Rac1-GTP localization in ruffles and at cell-to-cell contact, respectively. Images *a* and *b* and *g* and *h* were respectively merged in *c* and *i* showing (*arrows* in *c*) the sites of co-localization of Rac1-GTP with F-actin and *i* the distribution of Rac1-GTP compared with total Rac-1. *e* and *f*, fixed and permeabilized cells were co-incubated with mAb anti-Ve-cadherin (*e*), which was stained by anti-mouse TRITC-IgG, and GST-PBD (*f*), which was stained by as above described. *Arrow* in *f* shows Rac1-GTP localization near a cell-cell junction identified by the presence of Ve-cadherin (*arrow* in *e*). *Bar,* 10 μm. This panel is representative of five experiments obtained with similar results.

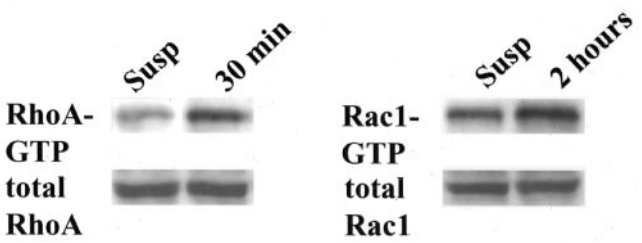

FIG. 4. **Pull-down assay in paraformaldehyde-fixed and permeabilized capillary ECs.** The amounts of RhoA-GTP and Rac1-GTP at 30 min and 2 h, respectively, of the morphogenetic process were evaluated as detailed in the legends of Figs. 2 and 3. Before cell lysis, ECs were fixed in paraformaldehyde and permeabilized in saponin (0.1%) as detailed under "Experimental Procedures." This panel is representative of two experiments obtained with similar results.

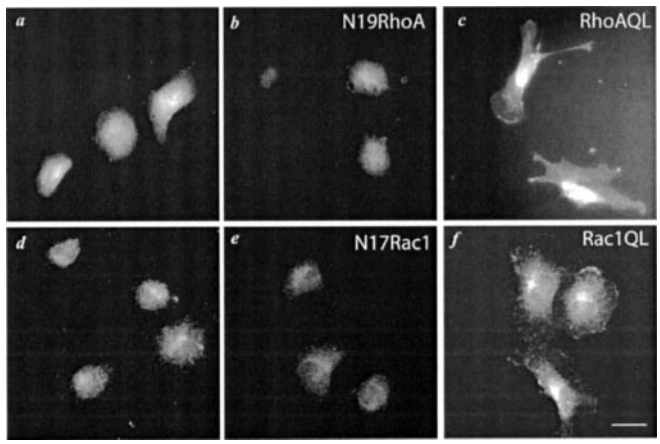

FIG. 5. **Immunolocalization of GST-RBD and GST-PBD in ECs carrying vector alone (*a* and *d*), N19RhoA (*b*), RhoAQL (*c*), N17Rac1 (*e*), and Rac1QL (*f*).** Cells were plated on gelatin-coated cover glasses, fixed, permeabilized, and incubated with GST-RBD (*a–c*) or GST-PBD (*d–f*) as detailed in legend to Fig. 2. *Bar*, 10 μm.

as paraformaldehyde is a cross-linking agent that may interfere in the stoichiometry of antigen-Ab interactions (43). The validity of this technique has been demonstrated previously in COS-7 cells carrying RhoQ63L, RacQ61L, and Cdc42Q61L (44), which respectively represent the constitutively active forms of RhoA, Rac1, and Cdc42 (36, 37).

To test the binding specificity of RhoA-GTP, Rac1-GTP to GST-RBD and GST-PBD, ECs cells were infected with Pinco vector carrying the constitutively active forms RhoAQL, Rac1QL, and the dominant negative mutants N17Rac1 and N19RhoA. RhoAQL (Fig. 5*c*) and Rac1QL (Fig. 5*f*) but not N19RhoA (Fig. 5*b*) or N17Rac1 (Fig. 5*e*), respectively, increased the staining of GST-RBD and GST-PBD. Anti-GST Ab did not detect any subcellular compartment (data not shown and see Ref. 44). No staining was detected following cell incubation with GST protein (data not shown and see Ref. 44). These data suggest that in our experimental conditions the intracellular immunostaining of GST-RBD and GST-PBD specifically tracks the localization of GTP-bound form of RhoA, Rac1 in ECs, as already reported in the nervous system (45).

In spreading ECs, 30 min after plating GST-RBD immunostaining showed predominant plasma membrane and perinuclear localization (Fig. 2*B*, *b* and *e*). At the plasma membrane level, RhoA-GTP concentrated at sites of membrane spreading and ruffling co-localizing with cortical F-actin (Fig. 2*B*, *c*). The GST-RBD immunofluorescence signal then became negative paralleling the low amount of RhoA-GTP detected in the pull-down assay (not shown). At 10 h EC-forming cords were characterized by few prominent stress fibers and by F-actin accumulation at cell-cell contacts (Fig. 2*C*, *a*). GST-RBD was found highly concentrated in areas near cell-cell contact and along the elongated body of the cell (Fig. 2*C, arrows* in *b, d,* and *e*). In these areas, it co-localized with F-actin (Fig. 2*C, arrows* in *c*). Fig. 2, *B, d,* and *C, f,* shows the distribution of RhoA, which appeared diffused in the cytosol and in the plasma membrane. Fig. 2, *B, f* and *C, h,* shows the merge between total RhoA and RhoA-GTP demonstrating that the active form was mainly concentrated in the plasma membrane 30 min after the beginning of morphogenetic process and in specific areas along the longitudinal cell axis after 10 h. In general this double staining suggests that only a fraction of RhoA becomes active and is recruited in discrete cell sites.

When RhoA was in active form (Fig. 2), Rac1-GTP was undetectable in agreement with the low levels of the active Rac1 measured in pull-down assay (data not shown and Fig. 3*A*). At 2 h, when Rac1 reached its activation peak, GST-PBD staining showed cytoplasm and plasma membrane positivity (Fig. 3*C*, *b*). Fig. 3*C* shows that Rac1-GTP concentrated in ruffles (*d*), at the edge of lamellipodia (*b*), and co-localized with cortical F-actin (*c*). Moreover, in early cell-cell contact events Rac1-GTP was near Ve-cadherin at cell-cell junctions (Fig. 3*C*, *e* and *f*, *arrows*). Active Rac1 *versus* Rac1 staining highlights the specific Rac1-GTP localization (Fig. 2*C*, *f*).

Subcellular localization analysis of Cdc42-GTP confirmed the data obtained by pull-down experiments, showing that GST-WBD staining was negligible in ECs (Fig. 3*B*) and did not co-localize with F-actin during vascular pattern formation (not shown).

Distinct Roles of RhoA and Rac1 during Capillary EC Morphogenesis—The observed differences in temporal activation profiles of distinct Rho GTPases as well as the different distribution of their GTP-bound forms suggested that they could play different functional roles in capillary network assembly. To gain insights into their functions, dominant negative mutants of Rac1 (N17Rac1), RhoA (N19RhoA), and Cdc42 (N17Cdc42) were expressed in capillary ECs through a GFP-retroviral vector (Fig. 6*B*, *insets*). To verify N17Rac1 and N19RhoA dominant negative activity, pull-down assays were performed when Rac1 and RhoA, respectively, reached its maximal activation level (Figs. 2*A* and 3*A*). Indeed, the amounts of Rac1-GTP at 2 h (Fig. 6*A*) and of RhoA-GTP at 30 min (not shown) and 10 h (Fig. 6*A*) were clearly reduced by the expression of the specific dominant negative mutants. Dominant activity of N17Cdc42 was not evaluated because the level of Cdc42-GTP did not change over time in our model. As shown in Fig. 6*B*, expression of both N19RhoA and N17Rac1 (Fig. 6*B*, *b* and *c*) impaired EC morphogenesis. The effect of N17Rac1 (Fig. 6*B*, *c*) was more dramatic with a relevant impairment of the initial phase when ECs migrate and establish cell-to-cell contacts generating cellular chains. The network formed by N19RhoA-ECs was less mature with evident interruption of cords (Fig. 6*B*, *b*). Quantification of capillary-like structures showed that the number of tubes were 123 $\pm$ 15/mm^2, 28 $\pm$ 7/mm^2, and 76 $\pm$ 8/mm^2 (mean $\pm$ S.D. of five experiments) in cells infected with the vector alone, N17Rac1, and N19RhoA, respectively. Capillary ECs expressing N17Cdc42 self-assembled into a mature vascular network without any morphological alteration (110 $\pm$ 5/mm^2 tubes; Fig. 6, *d*). The role of RhoA and Rac1 was further evaluated in an *in vitro* angiogenesis assay, in which ECs were aggregated into spheroids, embedded in type I collagen, and stimulated by VEGF-A$_{165}$. Fig. 6*C* shows that VEGF-A$_{165}$ elicited sprouting of capillary ECs from spheroids and that both N17Rac1 and N19RhoA impaired this phenomenon.

To exclude any possible interference of these GTPase mutants in the cell cycle that could influence the morphogenetic

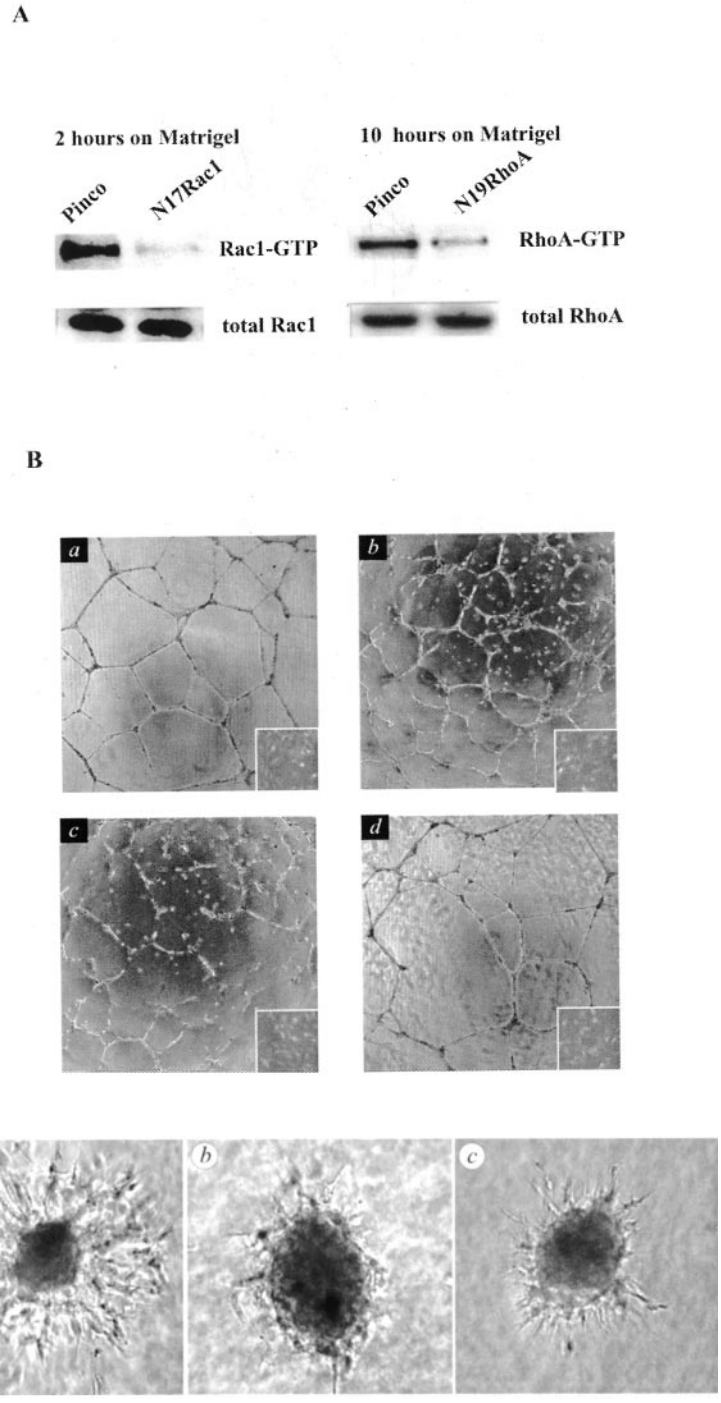

FIG. 6. **Effect of the expression of the dominant negative molecules N19RhoA, N17Rac1, and N17Cdc42 on capillary EC morphogenesis.** Capillary ECs were infected with Pinco retroviral vector carrying GFP and the specific mutated cDNA. Vector expression was evaluated by immunofluorescence detection of GFP on subconfluent ECs grown on plastic surface (*insets*). *A*, effect of N19RhoA and N17Rac1 expression on endogenous enzyme activities determined by pull-down assays as detailed in Fig. 2. Cell lysates were collected after 2 and 10 h, when RhoA and Rac1 activity peaked (see Figs. 2*A* and 3*A*). *B*, effect of the expression of Pinco vector (*a*), N19RhoA (*b*), N17Rac1 (*c*), and N17Cdc42 (*d*) on EC morphogenesis recorded after 14 h. *C*, effect of the expression of Pinco vector (*a*), N19RhoA (*b*), N17Rac1 (*c*) on EC sprouting induced by VEGF-A_{165}. ×100 magnification; *bar*, 10 μm. This panel is representative of three experiments obtained with similar results.

process *per se*, the apoptotic rate was evaluated 10 h after the beginning of the Matrigel assay. As also observed with ECs grown on plastic dishes (not shown), the expression of these mutants did not alter the number of apoptotic cells, which normally appear during *in vitro* angiogenesis (46, 47) (percentage of annexin V-positive cells: Pinco cells, 8.21 ± 3.20; N17Rac1-cells, 9.11 ± 2.67; N19RhoA, 7.89 ± 1.41; N17Cdc42-cells, 9.31 ± 2.60: mean ± S.D. of three experiment).

RhoA and Rac1 Regulate Key Biological Functions Required for Capillary EC Morphogenesis—We evaluated how Rac1 and RhoA could regulate key biological function required for the execution of a proper vascular morphogenetic process (7, 48) such as EC adhesion, migration toward Matrigel, and gel contraction (Fig. 7). We found that N17Rac1 did not affect EC adhesion to Matrigel (Fig. 7*A*, *a* and *d*), and expression of N19RhoA caused only a little reduction in the number of adhering ECs (Fig. 7A, *a*) even if it severely impaired the spreading of adherent ECs plated on Matrigel (Fig. 7*A*, *c*). Both N17Rac1 and N19RhoA reduced EC haptotaxis toward Matrigel, the former being more active (Fig. 7*B*).

ECs transduced with the vector alone contracted the Matrigel of 35%, and this effect was strongly reduced by cytochalasin D, an inhibitor of actin polymerization, and Y-27632, an inhibitor of the RhoA effector Rho kinase. These data suggest that Matrigel contraction requires tension generated by actin-myosin contractility (Fig. 7*C*). These inhibitors blocked also the formation of the tubule-like structures of the ECs (data not shown). Both N17Rac1 and N19RhoA reduced the capacity of ECs to contract the Matrigel, N19RhoA being more active (Fig. 7*C*). The effect of N19RhoA on gel contraction did not depend

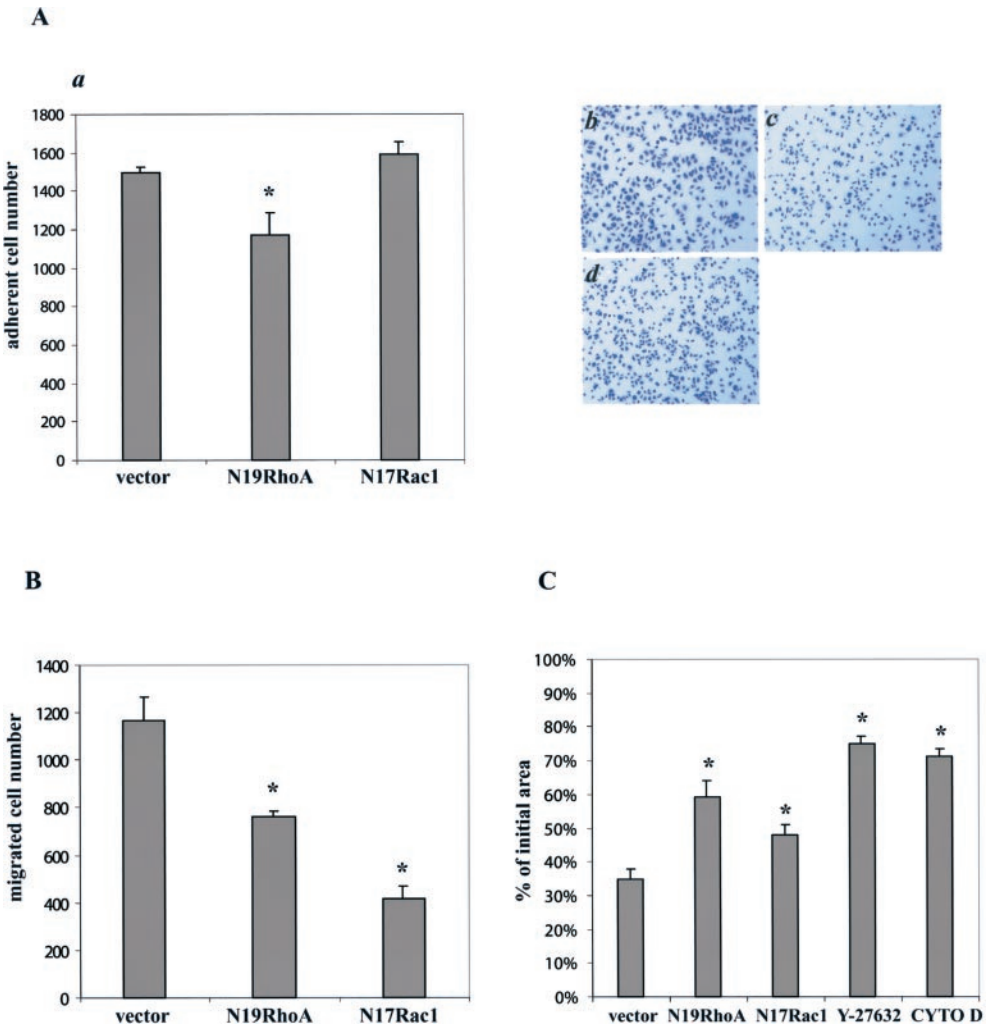

FIG. 7. **Adhesion, motility, and Matrigel contraction of ECs carrying N19RhoA and N17Rac1.** *A*, *a*, 10×10^4 ECs carrying vector, N19RhoA, or N17Rac1 were plated on 1.28 μg/μl Matrigel for 30 min. Adhered cells were fixed and stained by crystal violet; the absorbance was read at 540 nm in a microtiter plate spectrophotometer and expressed in number of cells. *Bars* indicate mean ± S.D. of four experiments done in duplicate. Data were analyzed by one-way analysis of variance ($p < 0.001$) and Student-Newman-Keuls test (* indicates $p < 0.05$ *versus* vector cells). Photographs of ECs carrying vector (*b*), N19RhoA (*c*), or N17Rac1 (*d*) stained by crystal violet are shown. ×100 magnification. *B*, 3×10^5 ECs carrying vector, N19RhoA, or N17Rac1 were allowed to migrate for 3 h in 24-well transwell chambers containing polycarbonate filters coated with 1.28 μg/μl of Matrigel. Migrated cells were stained by crystal violet; the absorbance was read at 540 nm in microtiter plate and expressed in number of cells. *Bars* indicate mean ± S.D. of three experiments done in duplicate. Data were analyzed by one-way analysis of variance ($p < 0.0001$) and Student-Newman-Keuls test (* indicates $p < 0.05$ *versus* vector cells). *C*, ECs (125 cells/mm^2) carrying vector alone or N17Rac1 or N19RhoA were plated on Matrigel in 24-well plates. In some experiments 5 μM Y27632 or 100 nM cytochalasin D was added. After 1 h, when cells spread, Matrigel was released from the underlying culture dish, and the contraction was allowed to proceed for 14 h. Matrigel contraction was analyzed by measuring the gel area, which was expressed as percentage of the initial area. *Bars* indicate mean ± S.D. of three experiments done in triplicate. Data were analyzed by one-way analysis of variance ($p < 0.0005$) and Student-Newman-Keuls test (* indicates $p < 0.05$ *versus* vector cells).

on the number of adherent cells because an increase of gel contraction was not observed even plating ECs carrying N19RhoA at higher concentration (not shown).

N17Rac1 Alters β-Catenin Localization—It is well established that Rac1 regulates homotypic cell contacts mediated by the cadherin-catenin complex (49). To evaluate the effect of N17Rac1 on adherens junction, we analyzed β-catenin and Ve-cadherin localization at cell-to-cell adhesion sites. In ECs infected with vector alone and plated for 2 h on Matrigel, β-catenin (Fig. 8*A*, *b*) and Ve-cadherin (data not shown) accumulated at cell-to-cell junctions. Capillary ECs expressing N17Rac1 showed a diffuse staining of β-catenin, which was not localized at intercellular contacts (Fig. 8*A*, *d*), whereas Ve-cadherin did (Fig. 8*A*, *f*). Small amounts of both β-catenin and Ve-cadherin was also seen in a punctate, vesicular pattern in the cytosol (Fig. 8*A*, *d* and *f*, *insets*).

Ve-cadherin forms intracellular complexes with β-catenin that recruits α-catenin, being responsible for actin cytoskeleton anchorage (50). The dynamics of the complex Ve-cadherin-catenins during the early steps of EC morphogenesis (30 min, 2 h) were evaluated by Western blotting analysis of proteins co-immunoprecipitated with β-catenin (Fig. 9*A*). In ECs carrying vector alone, Ve-cadherin co-immunoprecipitated with β-catenin heavily increased at 2 h compared with 30 min. α-Catenin was already complexed with β-catenin at 30 min, and the amount recruited to the complex slightly increased after 2 h. The expression of N17Rac1 did not modify the dynamics of the complex, suggesting that Rac1 inhibition did not impair cadherin-catenins interactions (Fig. 9*A*). Furthermore, we looked at the presence of IQGAP1 in the complex. This is a Rac1 effector that in the absence of active Rho GTPases may induce the dissociation of α-catenin from β-catenin (51, 52). In vector-ECs or N17Rac1-ECs, IQGAP1 is barely detectable in total cell lysate but was completely absent in β-catenin immu-

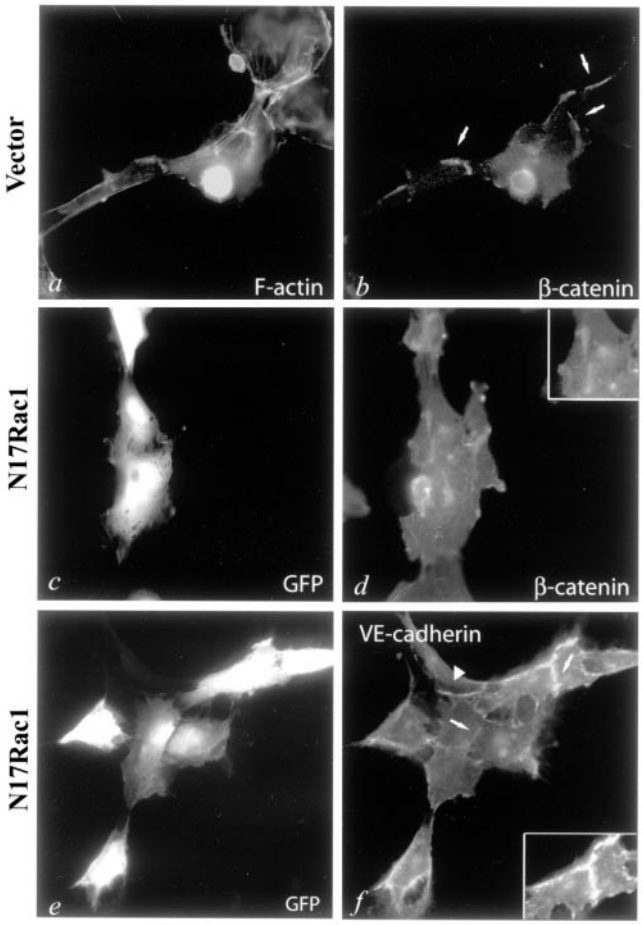

FIG. 8. **Effect of the expression of the dominant negative molecule N17Rac1 on β-catenin and Ve-cadherin localization.** ECs were infected with Pinco alone without GFP (*a* and *b*) or vector encoding N17Rac1 (*c–f*) plated on Matrigel, fixed, and permeabilized after 2 h. F-actin was stained with FITC-phalloidin (*a*), β-catenin (*b* and *d*), and Ve-cadherin (*f*), respectively, with mAbs anti-β-catenin and anti-Ve-cadherin followed by an anti-goat or anti-mouse TRITC-IgG. *c* and *e* illustrate GFP fluorescence of N17Rac1 cell expression. *b, arrows* indicate the localization of β-catenin at cell-cell junctions of ECs carrying vector alone. β-Catenin disappears in cells expressing N17Rac1 (*d*). *Arrows* in *f* indicate the localization of Ve-cadherin at cell-cell junction of ECs expressing N17Rac1, which did not change as compared with ECs not infected (*arrowhead*) or capillary ECs (see Fig. 3*C*, *e*). *Insets* in *d* and *f* show that small amounts of β-catenin (*d*) and Ve-cadherin (*f*) were present in a punctate, vesicular pattern. *Bar*, 10 μm. This figure is representative of four experiments obtained with similar results.

noprecipitates (Fig. 9*A*) suggesting that IQGAP1 is not involved at these stages of EC contact formation.

Association of cadherin-catenin complexes with actin cytoskeleton provides strength to adhesion (53). We then investigated the association of the Ve-cadherin complex to actin cytoskeleton analyzing the Triton X-100-insoluble fraction, as detergent insolubility is an indicator for cytoskeletal association (54). In ECs carrying vector alone, we observed an increase of Ve-cadherin and β-catenin amounts in the Triton X-100-insoluble fraction of cell lysates at 2 h compared with 30 min (Fig. 9*B*). N17Rac1 partially blocked this shift suggesting that in N17Rac1-ECs cadherin/catenin association to actin cytoskeleton was impaired. To test if the inhibitor effect of N17Rac1 may result from the perturbation of actin dynamics during new ECs contact formation, we looked at actin reorganization at sites of initial cell-cell contacts of ECs carrying N17Rac1. Non-infected ECs showed actin cables perpendicular to the cell-cell contacts, whereas poor actin reorganization and less cable protrusions were observed in N17Rac1 ECs (Fig. 9*C*). Morphometric analysis performed on 50 cell clusters containing at least one GFP-positive cell carrying the N17Rac1 and one GFP-negative cell indicates that 38.6 ± 5.3% (mean ± S.D. of four experiments) of the N17-Rac1 showed the absence of F-actin cables perpendicular to the nascent adherens junctions.

Because N17Rac1 affected the Ve-cadherin compartmentalization from soluble to insoluble Triton X-100 fraction, we performed a cell dissociation assay to determine cell adhesion activity of Ve-cadherin under conditions of high confluence when cell-cell junctions become mature. Confluent ECs carrying vector alone or N17Rac1 were treated with trypsin in the presence of Ca^{2+} or EGTA (TC or TE treatment), which respectively favor dissociation of EC monolayer in cluster or single cells (42). The ratio between the number of clusters (N_{TC}) and that of single cells (N_{TE}) was calculated (Fig. 9*C*). Because cadherin-mediated adhesion is reserved after TC but not TE treatment, smaller index reflects stronger adhesion activity. Both ECs carrying vector alone and N17Rac1 showed a similar N_{TC}/N_{TE} index. These results suggest that N17Rac1 effects could be rescued in mature cell-cell contacts of long confluence grown ECs.

MLC Is an Effector of RhoA at Specific Time Points of Capillary EC Morphogenesis—Because RhoA controls cell contraction by regulating the phosphorylation state of MLC (55, 56), we analyzed in N19RhoA-ECs the level of MLC-P and its cell localization by biochemical and immunofluorescence approaches.

At late stages of the vascular morphogenetic process (10 h), ECs showed an intense staining for MLC-P with focal accumulation at the periphery of the cell in the proximity of cell-to-cell contacts where it co-localized with F-actin (Fig. 10*A*, *a* and *b*). In contrast, in N19RhoA expressing ECs, the intensity of MLC-P staining was dramatically decreased and exhibited a diffuse cytoplasmic pattern (Fig. 10*A*, *c* and *d*). Because ECs expressing N17Rac1 did not form stretched cords (Fig. 6*B*, *c*), the pattern of MLC-P distribution was not compared with that of ECs carrying vector or N19RhoA. The effect of N19RhoA expression on the phosphorylation status of MLC was further validated by Western blot analysis on lysates from ECs plated on Matrigel for 30 min and 10 h, *i.e.* the time points when RhoA reached its maximal activation during *in vitro* vascular morphogenesis. MLC-P levels were clearly reduced in N19RhoA ECs when compared with N17Rac1 or vector alone infected cells (Fig. 10*B*).

DISCUSSION

We investigated the role of Rho GTPases during vascular network formation by human capillary ECs plated on a Matrigel scaffold. For the first time, we show here that Rac1 and RhoA are activated at specific time points during this morphogenetic process; we demonstrate that Rac1 is implicated in the early phases when EC migration and cell-to-cell contact formation occur, whereas RhoA is required for generating contractile forces during the remodeling phase.

Time-lapse analysis of the vascular morphogenetic process shows that a spread bidimensional multicellular network, whose geometry is not substantially modified in the following steps, forms during the first 2 h and undergoes complete maturation at later time points. Establishment of the primitive network is characterized by cell migration and maturation of cell-to-cell and cell-to-matrix interactions (7, 13, 48, 57). During this period two peaks of Rho GTPase activation are evident. RhoA-GTP is maximally activated at a very early stage, when ECs start adhering to Matrigel. The increase in Rac1-GTP levels occurs later, when ECs migrate and form Ve-cadherin-based cell-to-cell adhesions. During the early phases of ECs morphogenesis, total RhoA is localized both in the perinuclear region and in ruffling plasma membrane of spreading ECs, but

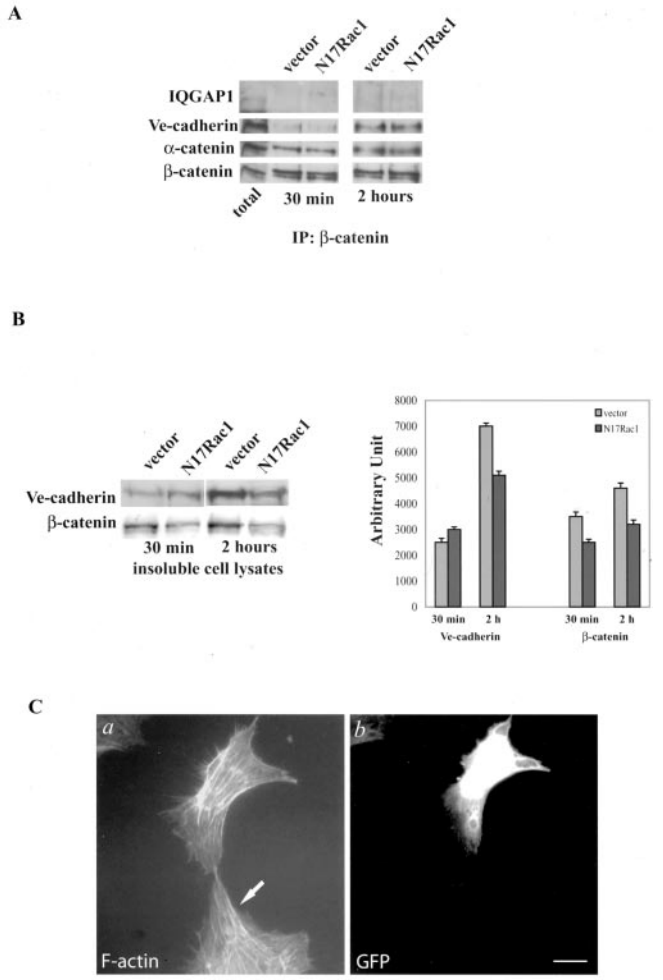

FIG. 9. **Effect of the expression of N17Rac1 on the dynamic of cell-to-cell adherens junctions.** *A*, capillary ECs carrying vector alone or N17Rac1 were plated on Matrigel and dispersed with MatriSperse cell recovery solution at 30 min or at 2 h from the beginning of the morphogenetic process, lysed, and immunoprecipitated (*IP*) with mAb anti-β-catenin. Proteins were separated by SDS-PAGE (8%) and then immunoblotted with Abs anti-IQGAP-1 and anti-α-catenin and mAbs anti-Ve-cadherin and anti-β-catenin. The total amounts in vector-ECs of the indicated proteins are shown in the *1st lane*. Equal results have been obtained in N17Rac1-ECs (not shown). *B*, ECs carrying vector alone or N17Rac1 were recovered as indicated above and lysed. After centrifugation, Triton X-100-insoluble pellets were solubilized in SDS buffer detailed under "Experimental Procedures" and boiled for 5 min. Solubilized proteins were separated on SDS-PAGE (8%) and immunoblotted with mAbs anti-Ve-cadherin or anti-β-catenin. Densitometric analysis of three independent experiments is shown as mean ± S.D. *C*, ECs carrying N17Rac1 were plated on Matrigel and after 2 h fixed and stained with TRICT-phalloidin (*a*). *b* shows the GFP expression in one of the two cells recorded in *a*. The negative GFP cell, which does not express N17Rac1, shows actin cable near and perpendicular to the cell protrusion forming the contact with a GFP-, N17Rac1-expressing cells. In this cell, F-actin is absent at the protrusion cone. Four experiments with similar results were performed. *D*, confluent cultured ECs carrying vector alone (*a*) or N17Rac1 (*b*) were treated with 0.01% trypsin in Hepes-buffered (TC treatment) or in Hepes-buffered saline without Ca^{2+} supplemented with 1 mM EGTA (TE treatment) for 15 min at 37 °C and dissociated through 10 times pipetting. The extent of dissociation cells was represented by the index N_{TC}/N_{TE}, where N_{TC} and N_{TE} are the number of clusters and single cells, respectively. This figure is representative of three experiments obtained with similar results.

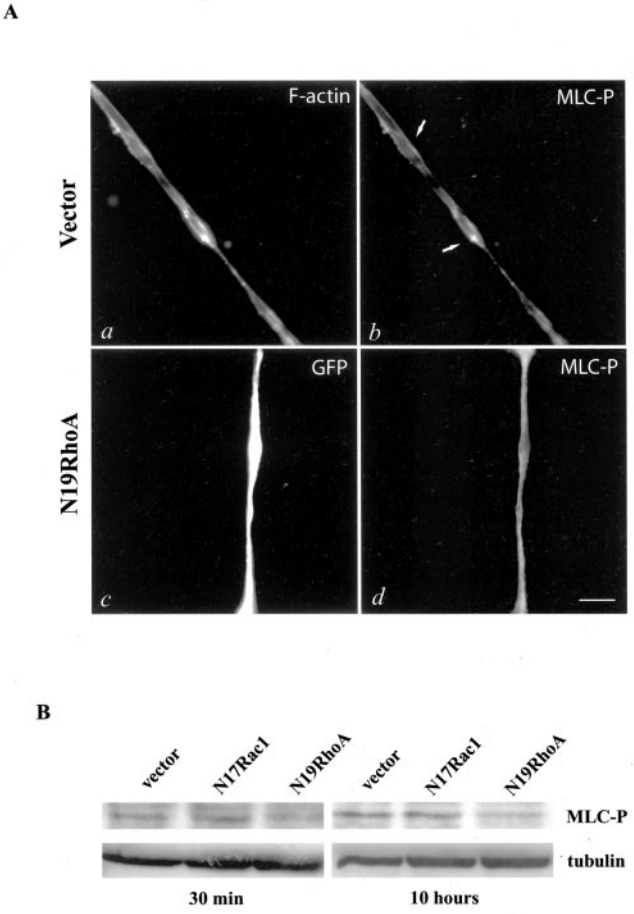

FIG. 10. **Effect of the expression of the dominant negative molecules N19RhoA on localization and phosphorylation of MLC.** ECs infected with vector alone, without GFP, or vector encoding N19RhoA were plated on Matrigel for 10 h. *A*, fixed and permeabilized cells were stained with FITC-phalloidin (*a*), and mAb anti-MLC-P followed by an anti-goat or anti-mouse TRITC-IgG (*b* and *d*). *c* illustrates GFP fluorescence in EC expressing N19RhoA. *Arrows* in *b* indicate the localization of MLC-P at the site of F-actin accumulation, which becomes more diffuse in cells expressing N19RhoA (*d*). *Bar*, 10 μm. *B*, Western blot analysis of MLC-P in ECs carrying N19RhoA and N17Rac1. After 30 min and 10 h from the beginning of morphogenetic process, ECs (1×10^6) were dispersed with MatriSperse cell recovery solution and lysed. Proteins were separated by SDS-PAGE (12%) and immunoblotted with a mAbs anti-MLC-P or anti-β-tubulin. This figure is representative of three experiments.

the GTP-bound form concentrates at membrane sites where it co-localizes with cortical F-actin. Total Rac1 is in cytosol, plasma membrane, and lamellipodia, whereas Rac1-GTP mainly co-localizes with F-actin in ruffles and lamellipodia plasma membrane and at cell-to-cell contacts of both ECs chains and clusters. The second stage of the morphogenetic process is primarily characterized by a remodeling of the network in which cells change shape to form capillary-like structures. During this latter phase, RhoA-GTP is augmented and co-localizes with F-actin containing structures, *i.e.* cell-to-cell junctions and stress fibers running along the longitudinal axis of ECs. Mobilization of Rho GTPases from cytosol to membranes has been described previously in polarized cells (17, 58) or after stimulation with platelet-derived growth factor, lysophosphatidic acid, and endothelia (59). However, this is the first demonstration that the GTP-bound form of Rho-GTPases may translocate in specific cell areas, including plasma membrane, during a morphogenetic process.

The use of dominant negative mutants N17Rac1, N17Cdc42, and N19RhoA allowed us to confirm the relevant role of Rac1 and RhoA in capillary network formation. The morphological features of the capillary network at the end of the morphogenetic process obtained with capillary ECs carrying dominant negative mutants indicate that inhibition of Rac1 exerts the

earliest and most dramatic effect with a profound alteration of the network. RhoA inhibition slightly compromises cell alignment along the geometric pattern. Cdc42 does not seem to play any role. These data are in contrast with a previous report (57) using a morphogenetic model in which human ECs from cord veins were plated in a tridimensional gel of collagen or fibrin. In this model Cdc42 is required as inferred by the use of a mutant molecule. However, it is well documented that the process of morphogenetic differentiation of ECs on collagen is completely dissimilar from that of ECs on Matrigel both in terms of temporal sequences of the process and types of integrin engaged (5, 6, 8, 60).

In vitro vascular network formation is a dynamic process characterized by three main stages: (i) adhesion to the extracellular matrix, (ii) movement on the extracellular matrix and formation of cell-to-cell contacts, and (iii) mechanical remodeling of the extracellular matrix by cell-generated tension force (7, 48, 61). N17Rac1 has a striking inhibitory effect on EC haptotaxis, whereas N19RhoA induces a slight inhibition of EC adhesion and motility but a more marked reduction of network remodeling and Matrigel contraction. Our observation that Matrigel contraction is impaired by inhibitors of Rho kinase (Y27632) and actin polymerization (cytochalasin D) suggests that it depends on actin-myosin contractility. Because RhoA is upstream RhoA kinase, we speculate that RhoA-GTP regulates vascular network remodeling through the control of actin-myosin contractility. Pharmacologically inhibiting Rho and RhoA kinase by using C3 exoenzyme and Y27632, respectively, Connolly *et al.* (13) did not notice any role of RhoA and actin-myosin contractility in the assembly of capillary-like structures. These discrepancies may be due to the different model they employed. Actually, the results by Connolly *et al.* (13) were obtained in an assay in which large vein ECs grown on glass surface were overlaid with Matrigel. On the contrary, our model focused on the ability of ECs adhering on Matrigel to undergo morphogenesis.

We found that when ECs are re-aligning to form chains, expression of N17Rac1 impairs β-catenin but not Ve-cadherin localization at intercellular junctions. By biochemical analysis of Ve-cadherin/catenins compositions, we have demonstrated that N17Rac1 does not modify the features of the complex during the early phases of vascular network formation. Similarly, Ve-cadherin ability to promote calcium-dependent cell-to-cell aggregation is not influenced by N17Rac1. However, the expression of this mutant does not allow the shift of Ve-cadherin-β-catenin complex to the Triton X-100-insoluble cellular fraction that contains cytoskeletal proteins (53). It has been reported that actin binding to the cadherin-β-catenin complex through α-catenin accounts for the shift of the junctional complex to cytoskeleton-associated detergent-insoluble structures (50, 54). Therefore, Rac1 seems to be crucial in allowing the association of Ve-cadherin-β-catenin complex to F-actin at adherens junctions in the early phases of vascular morphogenesis. This conclusion is also supported by immunofluorescence evidence that F-actin is absent at cell-to-cell contact in ECs expressing N17Rac1, and by previous observations (62) that a Ve-cadherin mutant lacking the last cytoplasmic amino acids was still able to support homotypic cell aggregation but was not able to provide cytoskeletal mediated strength to the junction. Therefore, ECs carrying N17Rac1 could arrest their morphogenetic process for the reduction of contractile forces generated during the formation of cell-cell contacts.

The role of Rac1 in controlling established Ve-cadherin/β-catenin-based cell-to-cell contacts in confluent ECs has been reported previously (24, 49, 63, 64) and seems to be largely dependent on the indirect regulation of the phosphorylation state of the complex. Actually, it has been reported that a constitutively active form of Rac1 induces a rapid loss of mature Ve-cadherin-mediated cell-to-cell contacts in confluent ECs concomitantly with an increase in tyrosine phosphorylation of α-catenin (64). Our data further extend the role of this GTPase to the early steps of cell junctions formation during *in vitro* angiogenesis in which Rac1 would regulate the connections between adherens junction and cytoskeleton.

Expression of N19RhoA leads to a dramatic reduction in MLC phosphorylation during the remodeling phase, when ECs assembled in stretched cords and stress fibers undergo orientation along the major cell axis. In control cells, MLC-P is mainly localized at cell-to-cell contact sites and along the major cell axis, whereas it is diffused in the cytosol of cells expressing the Rho mutant. Such MLC-P distribution is likely to be crucial for the control of tension driving forces within ECs during the remodeling phases. The residual MLC-P detected could be due to the activation of MLC kinase by the Ca^{2+}/calmodulin system (65). In muscle and non-muscle cells, inhibition of myosin phosphatase and the activation of Rho kinase, both regulated by RhoA, play a central role in MLC phosphorylation as well as in the assembly of stress fibers, focal adhesions, and in cell contraction and locomotion (19, 55, 56, 66, 67). Alteration of MLC-P in ECs carrying N19RhoA may in part explain their reduced ability to migrate on Matrigel and to contract the gel. Indeed actomyosin filaments provide the driving force for cell rear retraction and for contractility (58). RhoA has been implicated in several contractile events (59) and participates in modulation of the endothelial barrier function through the regulation of cytoskeletal tension (60). Nevertheless, examples of the generation of isometric tension in physiological morphogenetic processes are still poorly described. Our data shed light on the role of RhoA and MLC as key players in the execution of the vascular morphogenetic program.

The role of RhoA and Rac1 in regulating the formation and the dynamics of cell-to-matrix and cell-to-cell adhesive interactions is well established (14, 49, 68). Here we have shown that the different phases of the morphogenetic process, according to which human capillary ECs plated on Matrigel self-assemble into a vascular network, require distinct spatial and temporal activation of Rac1 and RhoA. Moreover, we have found that, during the different phases of this vascular morphogenetic process, the dynamics of nascent cell-to-cell adhesive contacts and MLC phosphorylation are major targets of Rac1 and RhoA.

REFERENCES

1. Guyton, A. C., and Hall, J. E. (eds) (2000) *Textbook of Medical Physiology*, 10th Ed., W. B. Saunders Co., Philadelphia, PA
2. Risau, W. (1997) *Nature* **386,** 671–674
3. Ingber, D. E., and Folkman, J. (1989) *Cell* **58,** 803–805
4. Bussolino, F., Mantovani, A., and Persico, G. (1997) *Trends Biochem. Sci.* **22,** 251–256
5. Montesano, R., and Orci, L. (1985) *Cell* **42,** 469–477
6. Grant, D. S., Tashiro, K., Segui-Real, B., Yamada, Y., Martin, G. R., and Kleinman, H. K. (1989) *Cell* **58,** 933–943
7. Folkman, J., and Haudenschild, C. (1980) *Nature* **288,** 551–556
8. Davis, G. E., and Camarillo, C. W. (1996) *Exp. Cell Res.* **224,** 39–51
9. Risau, W., and Flamme, I. (1995) *Annu. Rev. Cell Dev. Biol.* **11,** 73–91
10. Djonov, V., Schmid, M., Tschanz, S. A., and Burri, P. H. (2000) *Circ. Res.* **86,** 286–292
11. Yamada, O., Abe, M., Takehana, K., Hiraga, T., Iwasa, K., and Hiratsuka, T. (1995) *Arch. Histol. Cytol.* **58,** 567–574
12. Warburton, D., Schwarz, M., Tefft, D., Flores-Delgado, G., Anderson, K. D., and Cardoso, W. V. (2000) *Mech. Dev.* **92,** 55–81
13. Connolly, J. O., Simpson, N., Hewlett, L., and Hall, A. (2002) *Mol. Biol. Cell* **13,** 2474–2485
14. Hall, A. (1998) *Science* **279,** 509–514
15. Menager, C., Vassy, J., Doliger, C., Legrand, Y., and Karniguian, A. (1999) *Exp. Cell Res.* **249,** 221–230
16. Nobes, C. D., and Hall, A. (1999) *J. Cell Biol.* **144,** 1235–1244
17. Kraynov, V. S., Chamberlain, C., Bokoch, G. M., Schwartz, M. A., Slabaugh, S., and Hahn, K. M. (2000) *Science* **290,** 333–337
18. Sells, M. A., Pfaff, A., and Chernoff, J. (2000) *J. Cell Biol.* **151,** 1449–1458
19. Miyazaki, K., Yano, T., Schmidt, D. J., Tokui, T., Shibata, M., Lifshitz, L. M., Kimura, S., Tuft, R. A., and Ikebe, M. (2001) *J. Biol. Chem.* **277,** 725–734

20. Paik, J. H., Chae, S., Lee, M., and Thangada, H. (2001) *J. Biol. Chem.* **276,** 11830–11837
21. Soga, N., Naga, N., McAllister, S., Cornelius, L., Teitelbaum, S. L., Dowdy, S. F., Kawamura, J., and Hruska, K. A. (2001) *Exp. Cell Res.* **269,** 73–87
22. Dormond, O., Foletti, A., Paroz, C., and Ruegg, C. (2001) *Nat. Med.* **7,** 1041–1047
23. Wojciak-Stothard, B., Potempa, S., Eichholtz, T., and Ridley, A. J. (2001) *J. Cell Sci.* **114,** 1343–1355
24. Braga, V. M., Del Maschio, A., Machesky, L., and Dejana, E. (1999) *Mol. Biol. Cell* **10,** 9–22
25. Essler, M., Amano, M., Kruse, H. J., Kaibuchi, K., Weber, P. C., and Aepfelbacher, M. (1998) *J. Biol. Chem.* **273,** 21867–21874
26. Vouret-Craviari, V., Boquet, P., Pouyssegur, J., and Van Obberghen-Schilling, E. (1998) *Mol. Biol. Cell* **9,** 2639–2653
27. Sander, E. E., van Delft, S., ten Klooster, J. P., Reid, T., van der Kammen, R. A., Michiels, F., and Collard, J. G. (1998) *J. Cell Biol.* **143,** 1385–1398
28. Manser, E., Leung, T., Salihuddin, H., Zhao, Z. S., and Lim, L. (1994) *Nature* **367,** 40–46
29. Reid, T., Furuyashiki, T., Ishizaki, T., Watanabe, G., Watanabe, N., Fujisawa, K., Morii, N., Madaule, P., and Narumiya, S. (1996) *J. Biol. Chem.* **271,** 13556–13560
30. Li, R., Debreceni, B., Jia, B., Gao, Y., Tigyi, G., and Zheng, Y. (1999) *J. Biol. Chem.* **274,** 29648–29654
31. Symons, M., Derry, J. M., Karlak, B., Jiang, S., Lemahieu, V., Mccormick, F., Francke, U., and Abo, A. (1996) *Cell* **84,** 723–734
32. Lim, L., Manser, E., Leung, T., and Hall, C. (1996) *Eur. J. Biochem.* **242,** 171–185
33. Obermeier, A., Ahmed, S., Manser, E., Yen, S. C., Hall, C., and Lim, L. (1998) *EMBO J.* **17,** 4328–4339
34. Feig, L. A. (1999) *Nat. Cell Biol.* **1,** E25–E27
35. Cutrupi, S., Baldanzi, G., Gramaglia, D., Maffe, A., Schaap, D., Giraudo, E., van Blitterswijk, W., Bussolino, F., Comoglio, P. M., and Graziani, A. (2000) *EMBO J.* **19,** 4614–4622
36. Rottner, K., Hall, A., and Small, J. V. (1999) *Curr. Biol.* **9,** 640–648
37. Scita, G., Tenca, P., Frittoli, E., Tocchetti, A., Innocenti, M., Giardina, G., and Di Fiore, P. (2000) *EMBO J.* **19,** 2393–2398
38. Primo, L., Roca, C., Ferrandi, C., Lanfrancone, L., and Bussolino, F. (2000) *Oncogene* **19,** 3632–3641
39. Roca, C., Primo, L., Valdembri, D., Cividalli, A., Declerck, P., Carmeliet, P., Gabriele, P., and Bussolino, F. (2003) *Cancer Res.* **63,** 1500–1507
40. Strasly, M., Cavallo, F., Geuna, M., Mitola, S., Colombo, M. P., Forni, G., and Bussolino, F. (2001) *J. Immunol.* **166,** 3890–3899
41. Kolodney, M. S., and Wysolmerski, R. B. (1992) *J. Cell Biol.* **117,** 73–82
42. Takeichi, M. (1977) *J. Cell Biol.* **75,** 464–474
43. Hannah, M. J., Weiss, U., and Huttner, W. B. (1998) *Methods* **16,** 170–181
44. Cascone, I., Audero, E., Giraudo, E., Napione, L., Maniero, F., Philips, M. R., Collard, J. G., Serini, G., and Bussolino, F. (2003) *Blood* **102,** 2482–2490
45. Li, Z., Aizenman, C. D., and Cline, H. T. (2002) *Neuron* **33,** 741–750
46. Ranta, V., Mikkola, T., Ylikorkala, O., Viinikka, L., and Orpana, A. (1998) *J. Cell. Physiol.* **176,** 92–98
47. Segura, I., Serrano, A., De Buitrago, G. G., Gonzalez, M. A., Abad, J. L., Claveria, C., Gomez, L., Bernad, A., Martinez-A, C., and Riese, H. H. (2002) *FASEB J.* **16,** 833–841
48. Vernon, R. B., and Sage, E. H. (1995) *Am. J. Pathol.* **147,** 873–883
49. Fukata, M., and Kaibuchi, K. (2001) *Nat. Rev. Mol. Cell. Biol.* **2,** 887–897
50. Lampugnani, M. G., Corada, M., Caveda, L., Breviario, F., Ayalon, O., Geiger, B., and Dejana, E. (1995) *J. Cell Biol.* **129,** 203–217
51. Kuroda, S., Fukata, M., Nakagawa, M., Fujii, K., Nakamura, T., Ookubo, T., Izawa, I., Nagase, T., Nomura, N., Tani, H., Shoji, I., Matsuura, Y., Yonehara, S., and Kaibuchi, K. (1998) *Science* **281,** 832–835
52. Fukata, M., Kuroda, S., Nakagawa, M., Kawajiri, A., Itoh, N., Shoji, I., Matsuura, Y., Yonehara, S., Fujisawa, H., Kikuchi, A., and Kaibuchi, K. (1999) *J. Biol. Chem.* **274,** 26044–26050
53. Kemler, R. (1993) *Trends Genet.* **9,** 17–21
54. McNeill, H., Ryan, T. A., Smith, S. J., and Nelson, W. J. (1993) *J. Cell Biol.* **120,** 1217–1226
55. Katoh, K., Kano, Y., Amano, M., Onishi, H., Kaibuchi, K., and Fujiwara, K. (2001) *J. Cell Biol.* **153,** 569–583
56. Totsukawa, G., Yamakita, Y., Yamashiro, S., Hartshorne, D. J., Sasaki, Y., and Matsumura, F. (2001) *J. Cell Biol.* **150,** 797–806
57. Bayless, K. J., and Davis, G. E. (2002) *J. Cell Sci.* **115,** 1123–1136
58. Michaelson, D., Silletti, J., Murphy, G., D'Eustachio, P., Rush, M., and M. R., P. (2001) *J. Cell Biol.* **152,** 111–126
59. Fleming, I., Elliot, C. M., and Exton, J. H. (1996) *J. Biol. Chem.* **271,** 33067–33073
60. Madri, J. A., and Basson, M. D. (1992) *Lab. Investig.* **66,** 519–521
61. Serini, G., Ambrosi, D., Giraudo, E., Gamba, A., Preziosi, L., and Bussolino, F. (2003) *EMBO J.* **22,** 1771–1779
62. Navarro, P., Caveda, L., Breviario, F., Mandoteanu, I., Lampugnani, M. G., and Dejana, E. (1995) *J. Biol. Chem.* **270,** 30965–30972
63. Lampugnani, M. G., Corada, M., Andriopoulou, P., Esser, S., Risau, W., and Dejana, E. (1997) *J. Cell Sci.* **110,** 2065–2077
64. van Wetering, S., van Buul, J. D., Quik, S., Mul, F. P., Anthony, E. C., ten Klooster, J. P., Collard, J. G., and Hordijk, P. L. (2002) *J. Cell Sci.* **115,** 1837–1846
65. Katoh, K., Kano, Y., Amano, M., Onishi, H., Kaibuchi, K., and Fujiwara, K. (2001) *J. Cell Biol.* **153,** 569–584
66. Sakurada, K., Seto, M., and Sasaki, Y. (1998) *Am. J. Physiol.* **274,** C1563–C1572
67. Matsumura, F., Ono, S., Yamakita, Y., Totsukawa, G., and Yamashiro, S. (1998) *J. Cell Biol.* **140,** 119–129
68. Sahai, E., and Marshall, C. J. (2002) *Nat. Cell Biol.* **4,** 408–415

Molecular Basis of Cell and Developmental Biology:

Temporal and Spatial Modulation of Rho GTPases during *in Vitro* Formation of Capillary Vascular Network: ADHERENS JUNCTIONS AND MYOSIN LIGHT CHAIN AS TARGETS OF Rac1 AND RhoA

Ilaria Cascone, Enrico Giraudo, Francesca Caccavari, Lucia Napione, Elisa Bertotti, John G. Collard, Guido Serini and Federico Bussolino

J. Biol. Chem. 2003, 278:50702-50713.
doi: 10.1074/jbc.M307234200 originally published online September 12, 2003